Silicene nanosheets intercalated in slightly defective epitaxial graphene on a 4H-SiC(0001) substrate

Filippo Fabbri, Manuela Scarselli, Naveen Shetty, Sergey Kubatkin, Samuel Lara-Avila, Mathieu Abel, Isabelle Berbezier, Holger Vach, Matteo Salvato, Maurizio de Crescenzi, et al.

Silicene nanosheets intercalated in slightly defected epitaxial graphene on a 4H-SiC (0001) substrate

Filippo Fabbri[a], Manuela Scarselli[b], Naveen Shetty[c], Sergey Kubatkin[c], Samuel Lara-Avila[c,d], Mathieu Abel[e], Isabelle Berbezier[e], Holger Vach[f], Matteo Salvato[b], Maurizio De Crescenzi[b] and Paola Castrucci[b,*]

[a]*NEST, Scuola Normale Superiore, Istituto Nanoscienze-CNR, 56127 Pisa, Italy*
[b]*Dipartimento di Fisica, Università di Roma "Tor Vergata", 00133 Roma, Italy*
[c]*Department of Microtechnology and Nanoscience, Chalmers University of Technology, 412 96 Gothenburg, Sweden*
[d]*National Physical Laboratory, Hampton Road, Teddington TW11 0LW, United Kingdom*
[e]*CNRS, Aix-Marseille Université, IM2NP, UMR 7334, Campus de St. Jérome, 13397 Marseille, France*
[f]*CNRS-LPICM, Ecole Polytechnique, IP Paris, 91128 Palaiseau, France*

Abstract

In the last years, epitaxial graphene (epi-Gr) demonstrated to be an excellent substrate for the epitaxial or intercalated synthesis of two dimensional (2D) materials. Among 2D materials, silicene has been for a long time a dream for the scientific community, for its importance both from fundamental and application point of view. Despite, the theoretical prediction of silicene energetic viability, experimentally it is not so simple to induce silicon to hybridize in sp^2 configuration. In this respect, the substrate proved to play a fundamental role in the Si atom absorption process, leading in case of metal substrates to a mixed phase formation. For van der Waals chemical inert substrates, instead, like highly oriented pyrolytic graphite and MoS_2, Si atom intercalation even at room temperature has been reported and associated to non-ideality of their surfaces. Interestingly, very recently it has been shown that hundreds of nanometer area quasi-free standing silicene can be grown on top an almost ideal epi-Gr layer synthesized on 6H-SiC substrate. In the present paper, using scanning tunneling microscopy and spectroscopy and Raman analysis, we demonstrate that a non-ideal (slightly defected) epi-Gr network obtained by thermal decomposition of Si-terminated 4H-SiC(0001) enables the Si atoms penetration forming intercalated silicene nanosheets at RT, thus opening a path toward controlling intercalated silicene nanosheet formation through pristine graphene defect concentration managing and silicene application in nanotechnology.

Keywords: 2D materials, Silicene, Graphene, Van der Waals heterostructure, Raman spectroscopy, scanning tunneling spectroscopy, scanning tunneling microscopy

*Corresponding author: Paola Castrucci, email: paola.castrucci@roma2.infn.it

Introduction

In the last decade, epitaxial graphene (epi-Gr) demonstrated to be an optimal substrate for the epitaxial or intercalated synthesis of two dimensional (2D) materials, like transition metal dichalcogenides, [1-3] 2D-nitrides [4, 5] and two dimensional metals. [6, 7] Indeed, exploiting graphene intercalation ability enabled the growth of 2D materials which are not easy to render 2D since such a form is not the most energetically stable or inherently modifies interacting with environment. In addition, vertical heterostructures constituted by two or more 2D materials attract much interest because of unprecedented interfacial interactions and promises of novel electronics and optoelectronics applications. Among substrates used to synthesize epi-Gr, SiC(0001) offers several technological advantages like uniform large-area control of graphene number of layers, easy intercalation of H or other atomic species to tailor the interactions between SiC and graphene enabling future potential integration in wafer-scale fabrication processes. As far as 2D materials concern, probably one of the most fascinating though elusive is silicene. Silicene consists of a honeycomb lattice of atoms with non-conventional sp^2 hybridization of Si atoms thus presenting unique conductive properties due to its massless fermion carriers, [8, 9] the possibility to engineer its small energy bandgap by doping, applying electric or magnetic fields and to exploit its abilities in vertical and/or all metal (e.g. graphene/silicene) devices. [10, 11] A huge effort has been reported to synthetize quasi-free-standing silicene on several metal [12-15] and inert (i.e. MoS_2, [16, 17], graphite, [18-20], epi-Gr [21, 22]) substrates, giving rise to debates on the real possibility to obtain an air-stable, large area extended silicene layer on such substrates. Indeed, large lattice parameter differences favor Si sp^3 cluster formation [18, 20-23] and a number of Si atom superstructures [12, 15, 24] while the character of outmost substrate atoms dictates the potential interaction with Si. [25, 26] In addition, several studies demonstrated Si atoms intercalation through the monoatomic carbon atom honeycomb network after a thermal treatment at high temperature [22, 27, 28] or even in case of room temperature (RT) growth, [20, 25] though theoretically unexpected. [24, 29] Defects of the honeycomb carbon atom monolayer have been suggested to be at the origin of the observed Si atom intercalation at RT based on scanning tunneling microscopy (STM), Raman spectroscopy and ab-initio theoretical predictions. In ref. [25], ab-initio molecular dynamics calculations showed that atomic vacancies on the epi-Gr/Ni(111) surface are necessary for Si intercalation at RT and that no ordered 2D Si nanosheet formation is possible due to the covalent bonds formed between Si and Ni atoms. Moreover, interestingly enough, upon Si deposition on a highly oriented pyrolytic graphite substrate (HOPG), the observation of the graphite G mode redshift associated with the appearance of a 538 cm^{-1} Raman peak has been ascribed to the tensile strain induced by silicene nanosheet formation under the outermost monoatomic carbon layer. [20] In this case, being HOPG a van der Waals structure, charge density calculations predicted that intercalated Si atoms presents no bonds with overlayer and downlayer carbon atoms. [20] In this scenario, slightly defected epi-Gr grown on SiC(0001) substrate looks the most promising substrate for intercalated silicene formation at RT, since epi-Gr is separated from the bulk by a carbon interface layer (hereafter called the buffer layer (BL)) which do not binds to epi-Gr thus promising to prevent intercalated Si

- BL carbon atoms strong interactions. Very recently, it has been reported that silicene sheets some hundreds of nanometers large exhibiting a Raman peak at 560 cm^{-1}, very close to the theoretical value of 570 cm^{-1} for free-standing silicene, have been obtained for very low Si coverages on epi-Gr grown on 6H-SiC(0001) substrates. [30] In this paper the authors indicate as one of the prerequisites for such a silicene growth, the use of an almost defect free epi-Gr substrate with a Raman D/G band intensity ratio being of 0.09. This claim opens the pathway towards obtaining continuous silicene layer on epi-Gr and looks to confirm the previous hints for obtaining the RT synthesis of intercalated silicene nanosheets through epi-Gr defects.

In the present work, we investigated the RT deposition of silicon atoms on epi-Gr layer on a 4H-SiC (0001) substrate using low energy electron diffraction (LEED), x-ray photoelectron spectroscopy (XPS), scanning tunneling microscopy (STM) and Raman spectroscopy. We first note the weakening of the typical (6√3x6√3)R30° LEED spots of the carbon buffer layer present between the epi-Gr and the Si-terminated SiC substrate, (while the (1x1) graphene spots remain unchanged). Secondly, we observe on the STM images the presence of nanometer sized clusters, appearing rather flat on top, and intercalated under the epi-Gr network. No hints of Si 3D clusters on the graphene surface are observed by STM. Raman spectroscopy shows three main modifications of the epi-Gr modes: the splitting of the G band, the increase of the intensity of the D/G ratio from the pristine epi-Gr values and shift and intensity decrease of the 2D mode. Moreover, no typical crystalline sp^3 Si Raman mode (located around 520 cm^{-1}) is recorded while a peak at 538.5 cm^{-1} is displayed. These indications suggest the formation of silicene nanosheets intercalated underneath the epi-Gr layer, which is locally affected by a tensile stress due to the presence of such 2D silicon nanosheets. The present outcomes are all consistent with the presence of defects (e.g. atomic vacancies, dislocations, step and graphene sheet edges, …) on the pristine epi-Gr network as measured by Raman spectroscopy revealing, a D/G band intensity ratio reaching values up to 0.25, i.e. a factor 3 higher than in the ref. 30 case. These results suggest a route to manage the RT synthesis of more extended silicene nanosheets under epi-Gr on SiC(0001) substrate.

Experimental

A High-Purity Semi Insulating (HPSI) 4H-SiC(0001) substrate from CREE with a doping level of N_D~ $1x10^{14}$ cm^{-3} was graphitized at 1680°C for 10 minutes in P=850 mbar Argon. [31]

Graphitized 4H-SiC(0001) samples were introduced in the ultra-high vacuum (UHV) chamber (base pressure low 10^{-10} Torr) and in situ cleaned by annealing at 400°C for 10 minutes. Si evaporation was performed by direct heating of a high-purity silicon (Sil'tronix ST[redacted] epi-Gr/4H-SiC(0001) substrate. The deposition was done at a constant rate of 0.02 nm/min (0.07 ML/min) monitored by a quartz balance (Inficon). Deposition was carried out keeping the substrate at room temperature (RT). LEED patterns were recorded in-situ before and after the Si deposition by using an Omicron reverse LEED.

Samples were studied in situ by XPS as well as by scanning tunneling microscopy and spectroscopy (STS). C 1s, Si 2p, and Si 2s XPS photoemission spectra were measured using a non-monochromatized [illegible] (1486.6 eV) and a double-pass CMA operating in retarding mode. The energy scale was calibrated with reference to the binding energy of the Si $2p_{3/2}$ peak from a clean Si(100) (2 × 1) reconstructed sample which has been set to 99.9 ± 0.9 eV with respect to the Fermi level. XPS spectra were analyzed using Fityk software. STM imaging was performed using an Omicron-STM system operating at RT, with electrochemically etched tungsten tips. The STM was calibrated with atomically resolved images of the bare highly oriented pyrolytic graphite surface. [18] All images were acquired in the constant current mode and were unfiltered apart from a rigid plane subtraction. The local electron density of states near the Fermi level were investigated by STS. During the acquisition, the tunneling current was registered as a function of the applied bias (I vs V), the feedback loop was disabled, the bias-voltage set at 0.14 V and the set-point current, which regulates the [illegible] during the voltage scan. I-V curves were collected over grids of points equally spaced on the scanned s[illegible] were averaged over a set of several curves. The differential conduction was obtained by performing a derivative procedure.

Ex-situ Raman spectroscopy and mapping were performed without capping the samples. The Raman analysis was carried out with a Renishaw Invia spectrometer equipped with a confocal optical microscope and a 532 nm excitation laser. The Raman spectrum are acquired with a 100X objective with a numerical aperture NA=0.9, a laser power of 1 mW and an acquisition time of 5 s. The laser spot diameter size is evaluated to be 800 nm.[32] The spectral resolution is 2 cm^{-1}.

Results

Figure 1 displays the LEED patterns of the pristine epi-Gr on 4H-SiC(0001) (hereafter indicated as SiC) and of the sample surface after the evaporation of 0.5 and 1 ML of Si. In Figure 1a the white and yellow arrows indicate the reciprocal unit vectors of SiC and epi-Gr, respectively. The network of epi-Gr is rotated by 30° with respect to the SiC ones. Around the Gr (1x1) spots there are the six fractional order spots belonging to a superstructure with (6√3x6√3)R30° periodicity. This is caused by the marked atomic displacements induced by the formation of a carbon underlayer (standardly named buffer layer (BL) or zero-layer graphene), with a fraction of C atoms covalently bound to the outermost Si-terminated SiC surface. [33] The higher intensity of the epi-Gr spots with respect to six-fractional order spots of the (6√3x6√3)R30° BL is ascribed to the presence of the top monolayer epi-Gr. [34] Figure 1b and 1c exhibit the LEED evolution as Si deposition takes place. By increasing the Si amount, the spots of the (6√3x6√3)R30° BL and those of the (1x1) SiC become fainter and fainter. The epi-Gr spots, though, remaining well visible, reduce their intensity, and suffer a broadening. This

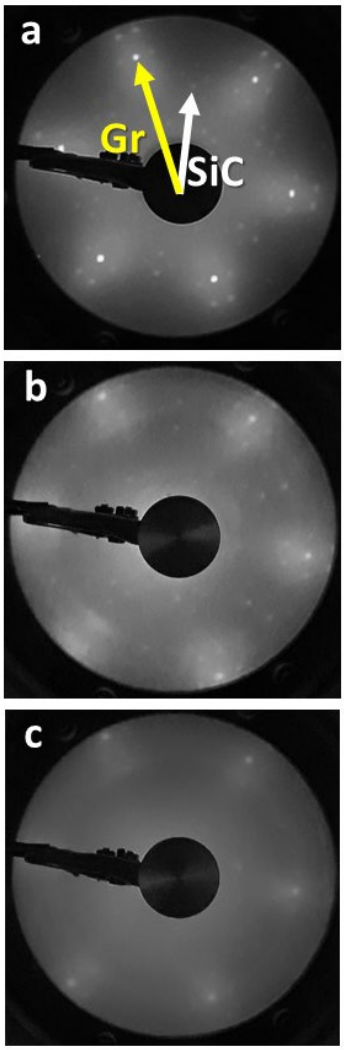

Figure 1 a. LEED pattern of the pristine epi-Gr on 4H-SiC(0001) after an annealing at 400°C for 10 minutes in UHV. The white arrow points to the reciprocal unit cell lattice parameter of 4H-SiC(0001) and the yellow one to the reciprocal unit cell lattice parameter of graphene, whose network is rotated by 30° with respect to the 4H-SiC(0001) ones. Around the graphene (1x1) spots there are the six factional order spots of the (6√3x6√3)R30° superstructure periodicity produced by the presence of the carbon atom buffer layer. b. LEED pattern after 0.5 ML Si deposition. c. LEED pattern for 1 ML Si coverage. Primary electron beam energy for all three LEED patterns is 63 eV.

indicates that the Si atoms degrade the crystallinity of the epi-Gr layer within a certain degree. For 3ML of deposited Si, the epi-Gr LEED spots also disappear behind a blurred background (data not shown). This can be interpreted as the loss of the epi-Gr long-range order and/or the formation of a few nanometer thick amorphous or short-range ordered 3D Si structures.

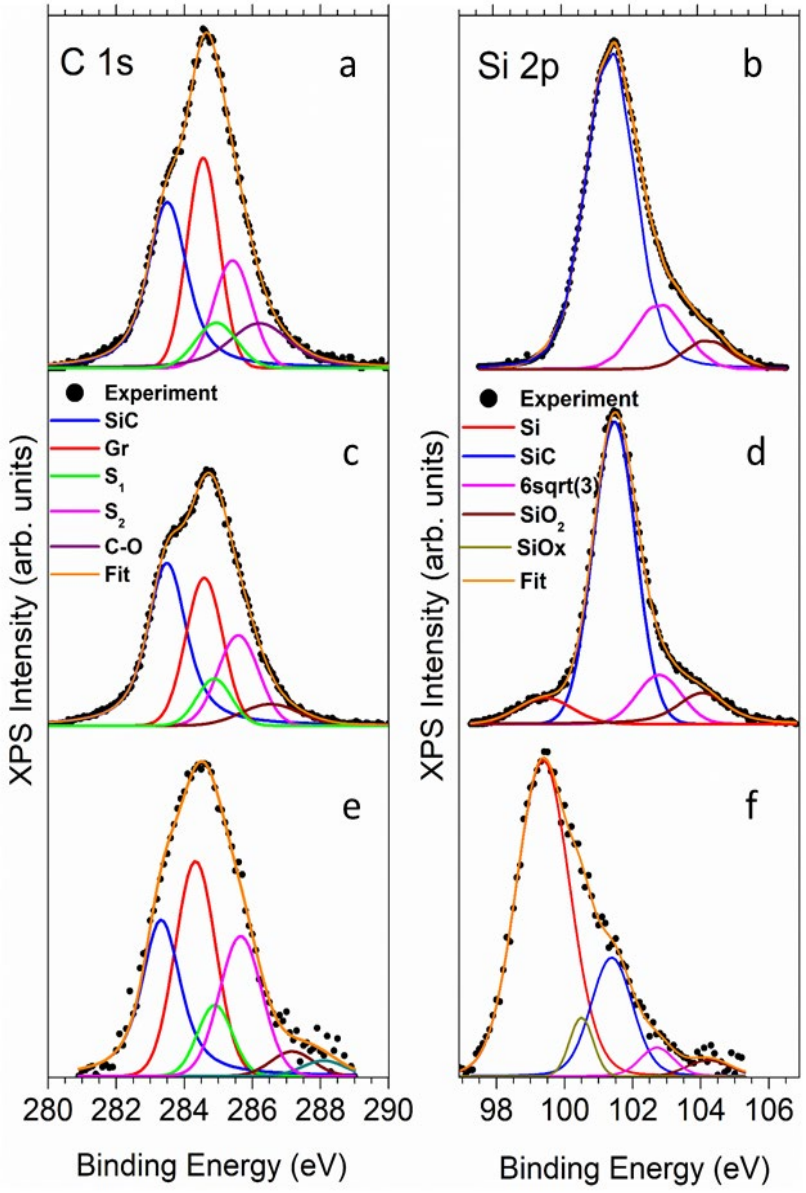

Figure 2 XPS spectra recorded at C 1s (left panel) and Si 2p (right panel) for the pristine epi-Gr on 4H-SiC(0001) (a,c); for the 1 ML (b,d) and 3 ML (e,f) of evaporated Si. The figures show the experimental data (black dots) and the constituent curves as resulting from a fitting procedure. The legends of the colored curves resulting from the fit procedure are reported in the figure.

Figure 2 reports the XPS spectra recorded at C 1s (left panel) and Si 2p (right panel) for the pristine epi-Gr on 4H-SiC(0001), the 1 ML and 3 ML of evaporated Si. XPS spectra have been arbitrarily normalized. The figures show the experimental data (black dots) and the curves resulting from a fitting procedure carried out after the Shirley background subtraction. In the case of Si 2p, due to the low XPS resolution induced by the use of the non-monochromatized X-ray source, the spin-orbit splitting was not accounted for. In Figure 2a, the C 1s

peak reveals the presence of a SiC (blue curve), epi-Gr (red curve) and two BL (green and magenta curves) components, named S_1 and S_2, respectively. The S_1 and S_2 components are due to the carbon atoms which are not bound (green curve) and bound (magenta curve) to the outermost Si atoms of the SiC substrate in accordance with the results reported in ref. [33]. In addition, a small contribution of the C-O feature (dark red curve) is also visible at 286.2 eV. The Si 2p shows the SiC component (blue curve), the one due to the Si atoms bound to the BL C atoms (magenta curve) and a weak SiO_2 peak. Silicon and carbon oxides were formed either during the graphitization process or during air exposure of epi-Gr defects. After 1 ML Si deposition, a small peak ascribed to Si-Si bonds (Figure 2d, red curve) appears in the Si 2p spectrum while the epi-Gr and the C-O features (Figure 2b, red and dark red curves) decrease in the C 1s one. These last findings indicate that Si mainly affects the epi-Gr layer and C-O bonds, while all the other C 1s components are preserved. This excludes the presence of thin (≤ 1-2 nm) Si structures on top of the epi-Gr layer, because in this case all the C 1s components would have their intensity reduced by the same factor. After the deposition of 3MLs of Si, the Si-Si peak dramatically increases (Figure 2f, red curve). At the same time, the C 1s spectrum (Figure 2e, blue curve) displays a huge reduction of the SiC component probably caused by the formation of thicker Si structures on the substrate surface. Such a high increase of the signal due to Si structures with respect to the one measured for the SiC substrate is consistent with the ratio between the area of the Si and C features obtained from the survey XPS spectra, which amounts to 0.27 for the pristine sample and increases to 0.31 and 0.60 after 1 ML and 3 ML Si deposition, respectively.

Figures 3a and 3b show the (150 nm x 150 nm) and the (40 nm x 40 nm) STM images of the epi-Gr/BL/4H-SiC(0001) surface after 1 ML Si evaporation at RT. Here and hereafter, the STM measurement parameters are reported in the figure captions. These images show the formation of nanostructures randomly distributed on the substrate terraces. The periodicity of the surface, not occupied by the islands, is 6X6, i.e. the same as observed on a pristine epi-Gr/BL/4H-SiC(0001) surface, with a superstructure distance of 1.65 ± 0.25 nm measured both on the line profile (Figure 3c) and on the two-dimensional Fast Fourier Transform (2D-FFT) reported in the inset of Figure 3a. This 6x6 corrugation is indeed often imaged by STM and reflects the presence of the (6√3x6√3)R30° superstructure imposed by the registry match of Si outermost atoms of the SiC and the carbon BL. [35] In our STM acquisition conditions, the apparent height modulation of the 6x6 superstructure amounts to about 0.1 nm, as reported in the literature. [35, 36] Some nanostructures appear very small, with a diameter around 1 nm, while others reach sizes up to 10 nm. The apparent nanostructure height ranges between 0.2 and 0.4 nm (see the line profile reported in Figure 3d). In addition, on the STM atomic resolution images, the graphene network is clearly visible everywhere (see Figure 4a, Figure 4b and Figure 4e), as also shown by the 2D-FFT reported in Figure 4c, Figure 4f and in Figure SM1 in the Supplementary Materials. All this suggests the intercalation of Si atoms at RT. Moreover, if we observe the STM high magnified images (Figure 4a and Figure 4b white square), the Si nanometric islands appear to be in

correspondence with the bumps of the (6x6) superstructure. This observation appears without ambiguity in the line profile reported in Figure 4d (see arrow). Figure 4b also shows a very large nanostructure which

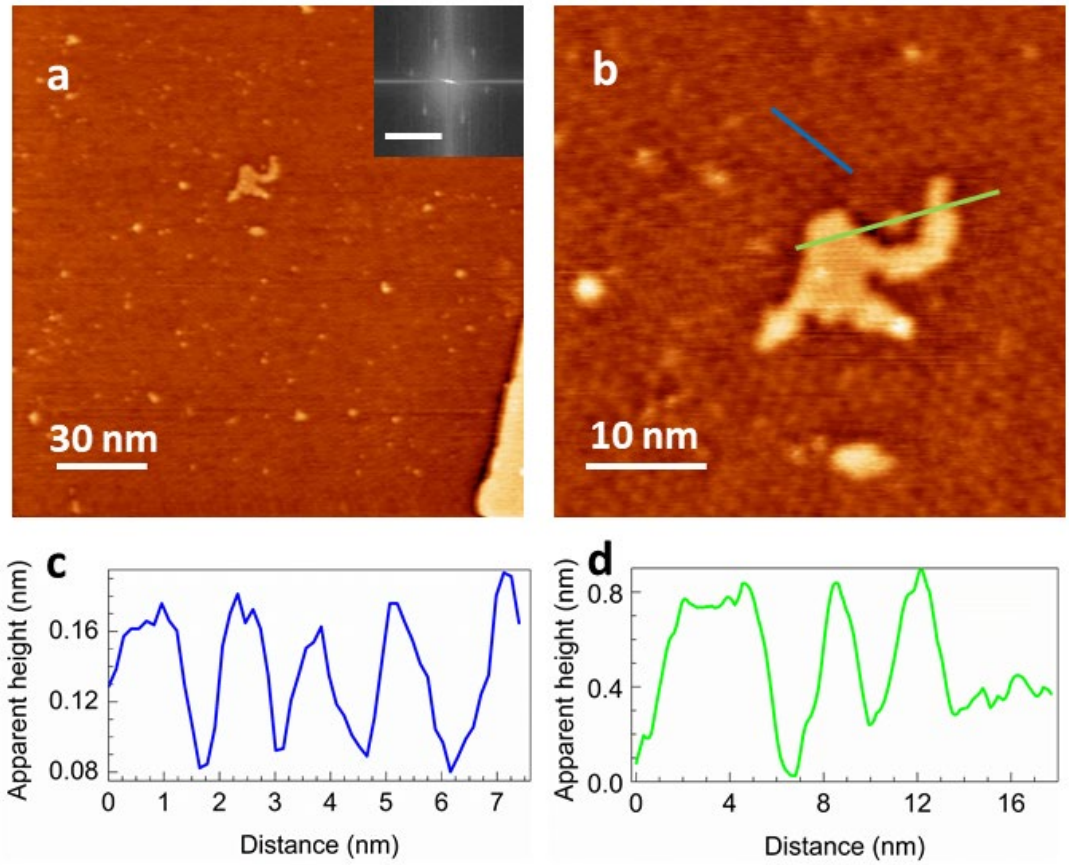

Figure 3 a, b: STM images of the Gr/BL/4H-SiC(0001) surface after 1 ML Si deposition at RT, (150 nmx150 nm) and (40 nmx40 nm) respectively. Bias voltage 0.8 V, feedback current 0.5 nA. The inset in panel a reports the 2D-FFT of the entire scanned surface, showing a hexagonal pattern with a lattice periodicity of 1.65 ± 0.25 nm, typical of the (6x6) superstructure observed on a bare Gr/BL/4H-SiC(0001) surface. The scale bar equals to 1 nm^{-1}. c: line profile measured along the blue line in b, showing the apparent height and lateral size of the (6x6) superstructure due to the BL. d: line profile measured along the green line in b, displaying the apparent height of the large nanostructure and isolated islands.

seems to be constituted by several touching and nanometer sized islands under the graphene network. This closeness of small nanostructures is also clearly displayed by the line profile (Figure SM2c) taken along the green line in Figure SM2a. Interestingly, the graphene network in Figure 4e appears partially distorted with the respect to the ideal one, probably due to the presence of a tensile stress experienced because of the Si underneath. This is also confirmed by the presence of elongated spots in the 2D-FFT reported in Figure 4c, hints of the existence of honeycomb lattice parameters a little bit different from that of the epi-Gr. In addition, the red arrow shows the presence of a dislocation in the graphene network suggesting that this could be the point defect enabling Si atom penetration under the graphene layer. In Figure SM3 are reported

two STM images of the pristine epi-Gr exhibiting defects presence both in the 6x6 periodicity of the BL and in epi-Gr network, thus indicating that the starting substrate is slightly defected.

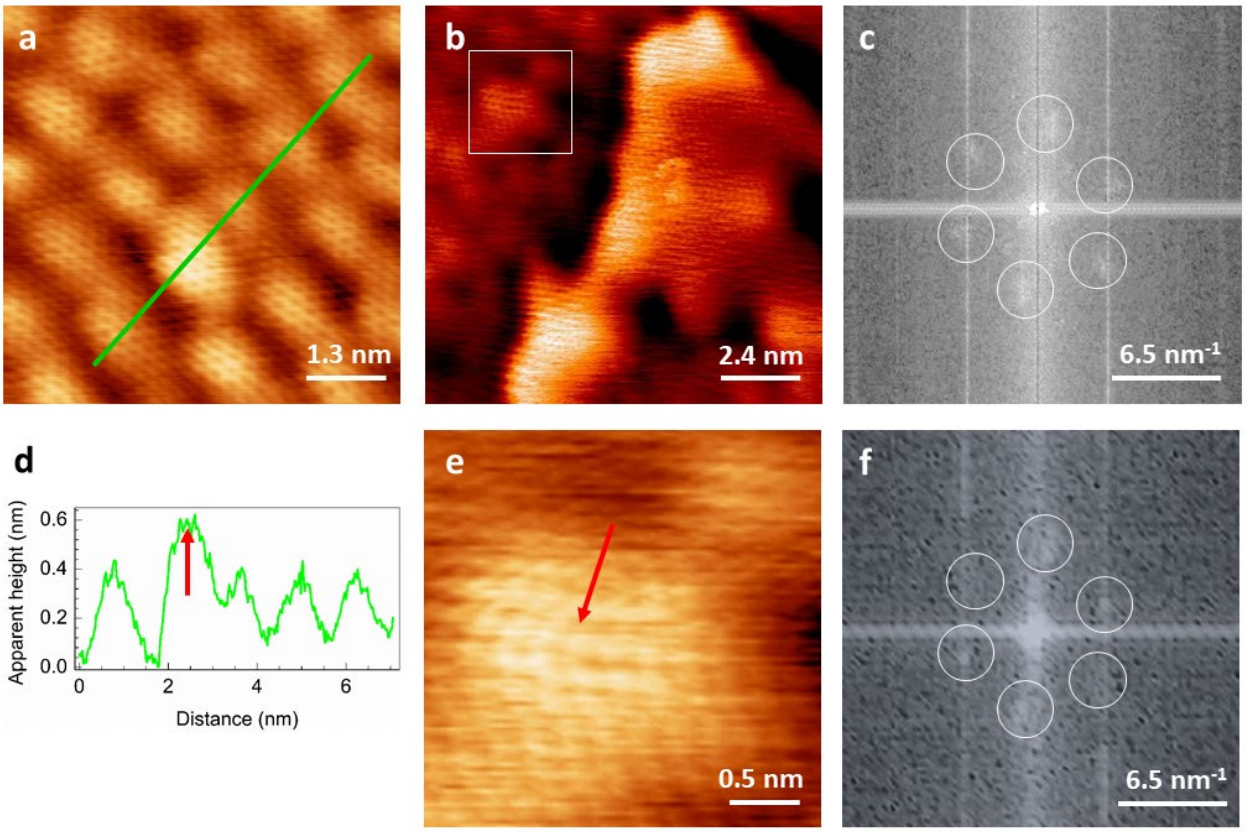

Figure 4 a: STM (6.5 nm x 6.5 nm) image of the epi-Gr/BL/4H-SiC(0001) surface after 1 ML Si evaporation at RT. It is worth noting the extra-protrusion induced by the Si atom intercalation located in one of the (6x6) BL bumps. Its apparent height is demonstrated by the line profile (green line) reported in d (see red arrow). Bias voltage 0.1 V, feedback current 0.36 nA. The scale bars are indicated on the image. b: STM (12 nm x 12 nm) image of the epi-Gr/BL/4H-SiC(0001) surface after 1 ML Si evaporation at RT, showing two nanostructures of different size. Bias voltage 0.17 V, feedback current 0.5 nA. c: 2D-FFT of the area imaged in b. Though faint, note the hexagonal pattern typical of the graphene honeycomb lattice and the elongation of the 6 spots suggesting the presence of several graphene lattice parameters, probably due to the strain suffered by epi-Gr as a consequence of intercalation. e: Zoom of the smaller nanostructure framed in the square white box in b, showing the graphene network and the presence of a dislocation indicated by the red arrow. f. 2D-FFT of the area zoomed in e, showing the presence of hexagonal pattern typical of the honeycomb network of graphene. The graphene network is visible in all areas scanned on the STM images in a and b. The apparent height of this nanostructure is reported in the line profile in SM2c.

Figure 5a reports the STM image of 3 ML Si deposited at RT on a epi-Gr/BL/4H-SiC(0001) surface. We observe that the entire surface is covered by three-dimensional (3D) islands of various sizes. The smaller ones (Figure 5b) have nanometric size (see line profile in Figure 5c) while the bigger ones result of an agglomeration of these nanometric islands (see line profile in Figure 5d). This means that by increasing the deposited Si amount, the formation of 3D island is becoming prevalent compared to the intercalation process, as was also observed in the case of Si on a graphite substrate. [20] Unfortunately, the atomic resolution of such islands was not reached in the high magnification STM images.

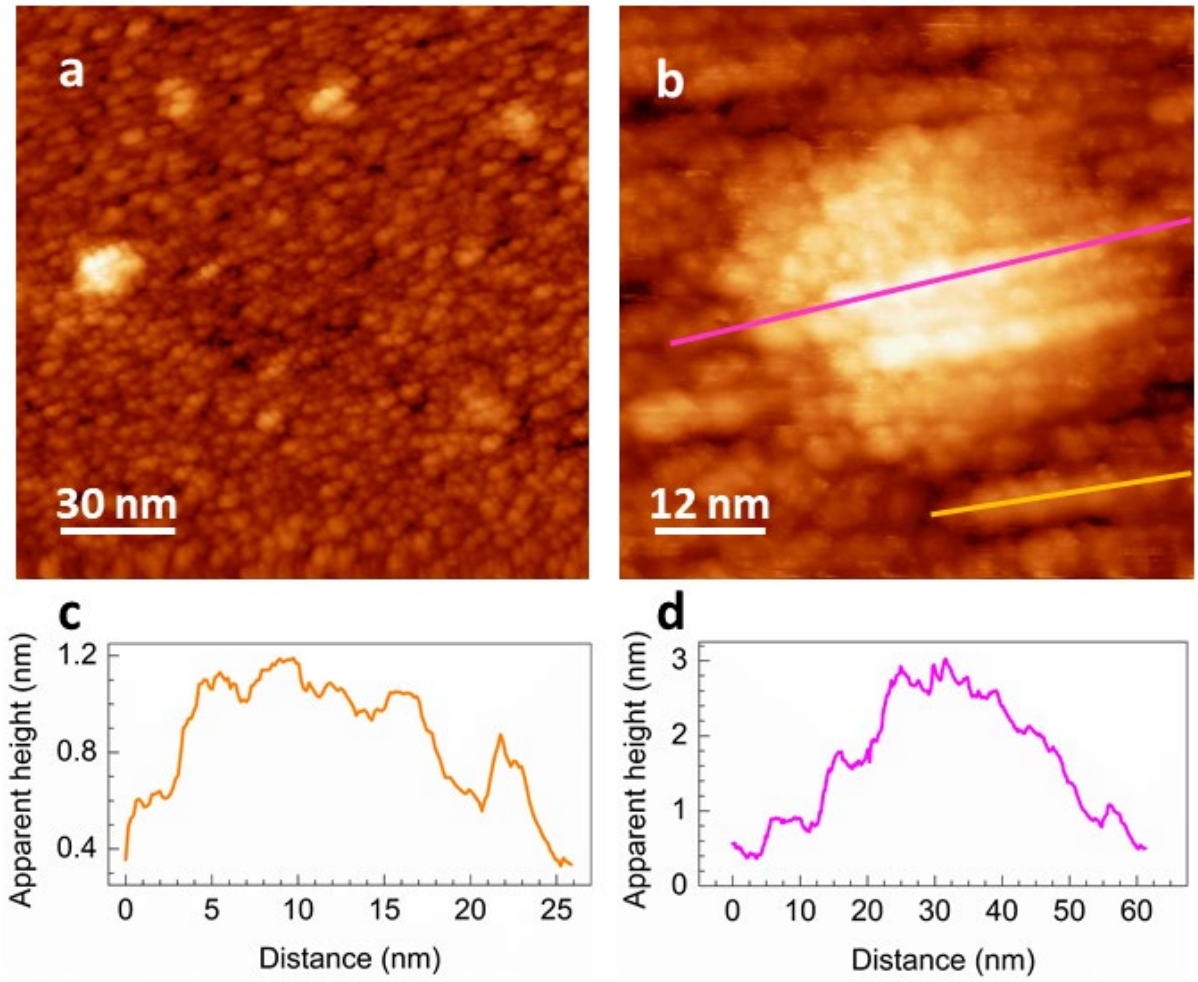

Figure 5 a: STM (150 nm x 150 nm) image of the Gr/BL/4H-SiC(0001) surface after 3 ML Si deposition at RT. The surface is covered by 3D Si islands of several sizes. Bias voltage 2 V, feedback current 0.3 nA. b: STM (60 nm x 60 nm) image of the Gr/BL/4H-SiC(0001) surface after 3 ML Si deposition at RT. The island appears as an agglomeration of smaller nanometric 3D Si islands, whose dimensions are demonstrated by the line profile taken along the orange line and displayed in c. Bias voltage 2 V, feedback current 0.3 nA. d: apparent height profile measured along the magenta line in b, exhibiting the lateral size of about 20-30 nm of these agglomerations and their apparent height of about 3 nm.

Figure 6 shows the STS differential conductance acquired for the same 1 ML Si sample on the epi-Gr (black curve), on the intercalated nanostructure (reported in Figure 4 on top of which a graphene network is visible on the surface, red curve) and on the 3D Si islands (blue curve) (reported in Figure 5). While the red curve recorded for 1ML of Si resembles closely the graphene metallic nature (black curve) due to the finite value around the Fermi level (e.g. around zero voltage value), the blue curve has a marked semiconductor behavior with a very low conductance. This dI/dV behavior confirms the hypothesis of Si intercalation under the graphene layer after 1ML Si evaporation. This suggests that the graphene electronic properties are not modified by the presence of silicon underlayer within the limitations of this STS technique performed at RT. This is a further hint of no interaction between the Si nanostructure and the graphene layer.

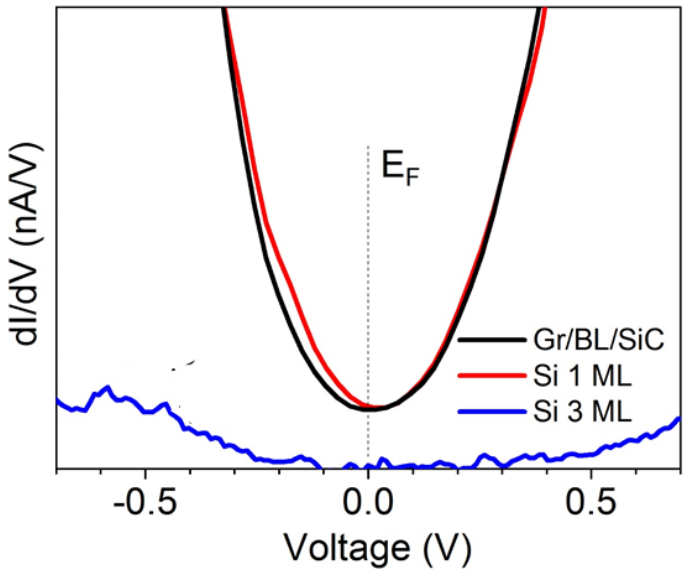

Figure 6 STS differential conductance recorded on the bare Gr/BL/4H-SiC(0001) surface (black curve), on an intercalated Si island (red curve) reported in Figure 4 and on a 3D Si island (blue curve) displayed in Figure 5. The first two curves show a metallic Dirac like behavior modulated by the Fermi Dirac function at room temperature, the blue one presents a semiconducting behavior confirming the Si sp^3 hybridization.

In Figure 7a the Raman spectra acquired in the silicon range (200-650 cm^{-1}) for the pristine epi-Gr sample (red curve), the 1 ML (green curve) and 3 ML (blue curve) of deposited Si show the typical Raman peak attributed to the 4H-SiC(0001) substrate located at 265 cm^{-1}. All the spectra have been renormalized to the 4H-SiC(0001) TO peak at 777 cm^{-1}, see the whole spectra in Figure SM4. After the deposition of 1 ML of Si a Raman mode appears at around 538 cm^{-1}, while in the 3 Si ML case, a similar Raman feature is found at 532 cm^{-1} together with a broad band, peaked at 470 cm^{-1}, that is most likely due to amorphous silicon. The Raman spectra of the 1ML and 3ML cases, where the pristine epi-Gr spectrum was subtracted, are reported in Figure SM5. Recently, a similar Raman mode, peaked at 542 cm^{-1}, has been reported for Si deposited at RT on a HOPG substrate. Based on a detailed theoretical calculation, this Raman mode was attributed to the formation of silicene nanosheets on the HOPG substrate. [19] A possible explanation to the shift of the silicene Raman mode can be due to the different doping caused by the intercalation in an epi-Gr substrate with respect to the HOPG substrate. It has been predicted by theoretical calculation that the doping (with electron or holes) affects the Raman shift position in the same way. [37] Therefore, considering the 5 cm^{-1} shift in case of the 1 ML silicon deposition it can be due to a doping of ±0.05 eV. While the shift of 10 cm^{-1} in case of the 3 ML silicon deposition could be the demonstration of doping of ±0.1 eV. We don't expect any particular strain related shift due to the similar nature in terms of lattice parameters between epitaxial graphene and HOPG. The histogram, reported in Figure 7b, displays the distribution of the intensity of the 2D silicon peak in case of 1 ML (green line) and 3 ML (blue line) silicon depositions on epitaxial graphene. For the 1 ML Si deposition the histogram presents a single peak distribution, while the 3 ML deposition case presents a three peaks distribution. This can be an indication that in the case of 1 ML deposition, silicene is mainly monolayer,

while, in case of the 3 ML silicon deposition, the formation of bilayer patches of silicene or the presence of areas with a higher silicene density become possible. Figure 7c and 7d show the Raman maps of the intensity of the 2D silicon mode for the 1 ML and 3 ML silicon deposition, respectively. The spatial distribution of the 2D silicon, in case of the 1 ML deposition, is randomly distributed, while for the 3 ML deposition, there is an indication that the bilayer islands or the areas with higher silicene density are formed along certain direction, most likely parallel to the step-edges of the SiC substrates.

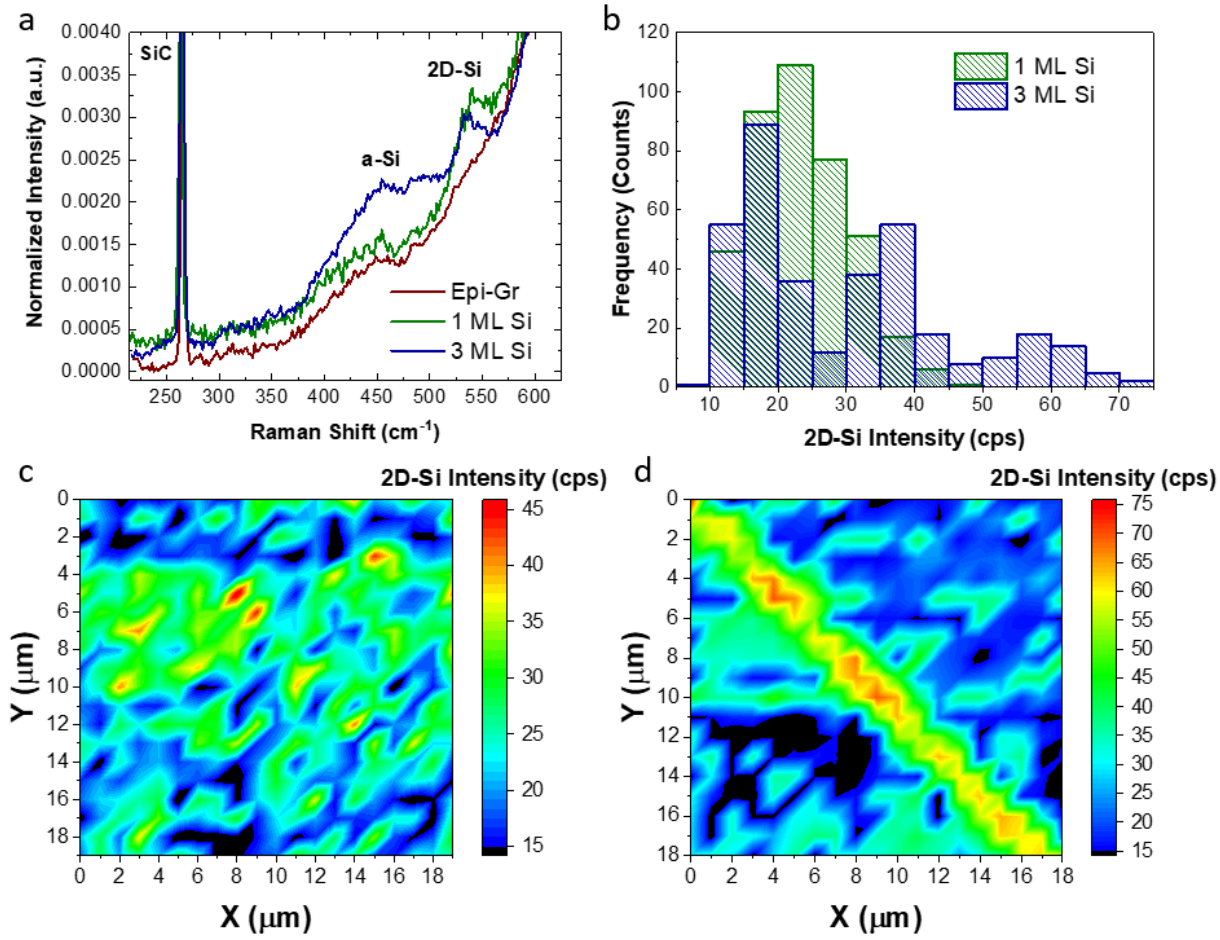

Figure 7 a: Raman spectra in the silicon range for the pristine epi-Gr/BL/4H-SiC(0001) (red curve), the 1 ML (green curve) and 3 ML (blue curve) of deposited Si. b: Histogram of the 2D Silicon Raman mode intensity c: 20 ⍰m x 20 ⍰m Intensity map of the 2D silicon mode after 1 ML deposition. d: 20 ⍰m x 20 ⍰m Intensity map of the 2D silicon mode after 3 ML deposition. Pay attention to the different color scale bar in c and d Raman maps.

By analyzing representative Raman spectra in the graphene range (Figure 8a), it is possible to highlight some strong modifications of the epitaxial graphene after the silicon deposition. It is worth noting that all the spectra are renormalized to the second-order peak of silicon carbide, peaked at 1516 cm^{-1}. The bare epitaxial graphene sample presents the 2D Raman mode as single Lorentzian peak, indication of single-layer graphene. [38,32] After the silicon deposition the 2D peak concurrently suffers a shift toward lower wavenumbers and a broadening, that monotonically increases with the number of deposited Si MLs. The 2D broadening as

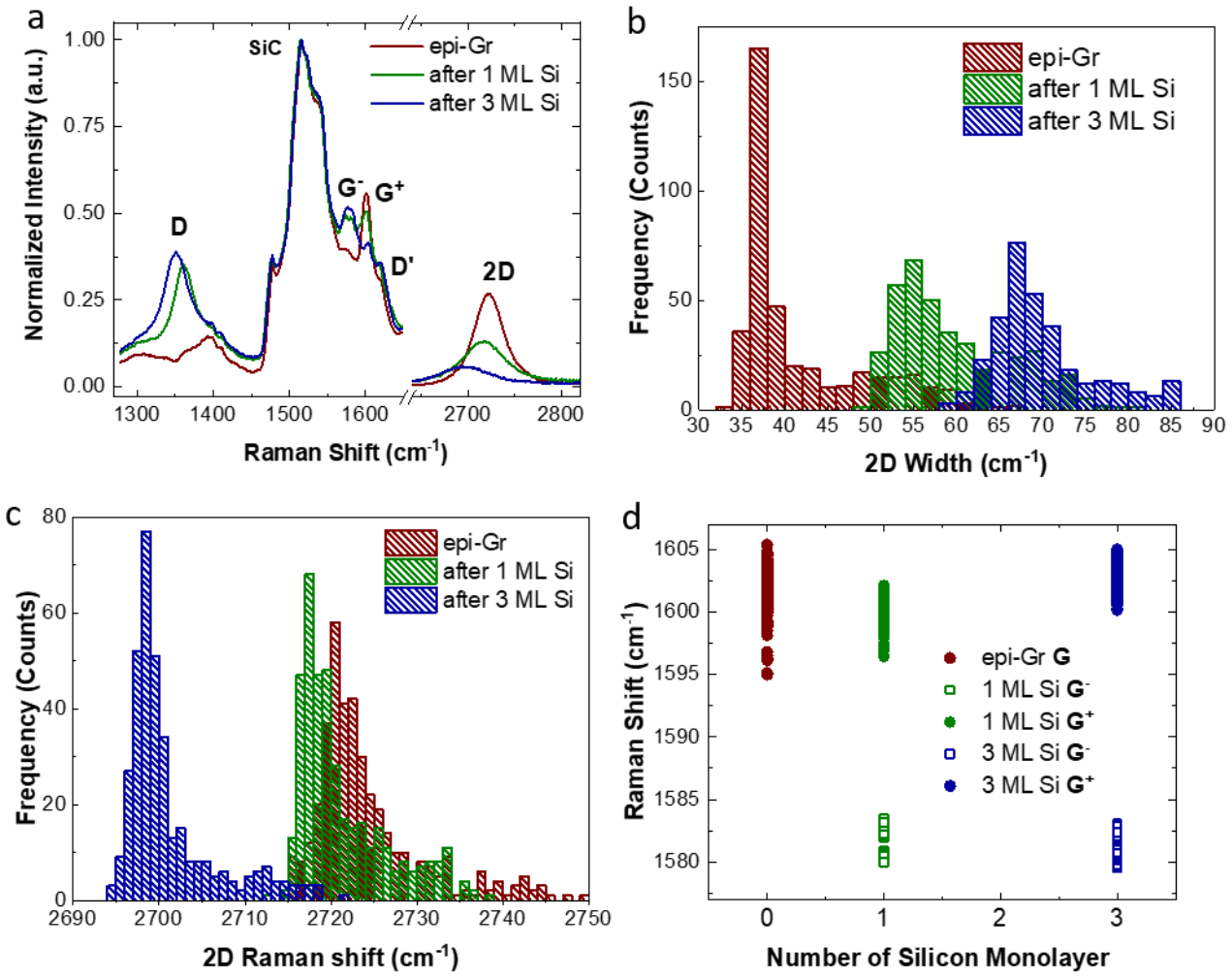

Figure 8 a: Raman spectra in the graphene range for the pristine epi-Gr/BL/4H-SiC(0001) (red curve), the 1 ML (green curve) and 3 ML (blue curve) of deposited Si. b: Histogram of the epitaxial graphene 2D Raman mode FWHM. c: Histogram of the epitaxial graphene 2D Raman shift. d: summary graph of the Raman shifts of the G Raman mode.

function of the number of Si MLs is clearly resumed in Figure 8b, where the histogram reveals that the bare epitaxial graphene has an average width of the 2D peak of 37.5 cm^{-1} (with a secondary peak at about 52.5 cm^{-1} due to bilayer epi-graphene) that increases up to 55 cm^{-1} in the case of 1ML Si deposition, reaching the maximum value of 67.5 cm^{-1} after the deposition of 3 ML of silicon. The shift of the 2D peak is statistically highlighted in Figure 8c, where the histogram reveals that the average 2D Raman shift in case of bare epitaxial graphene is peaked at 2721 cm^{-1}, and it decreases down to 2718 cm^{-1} for 1 ML Si deposition, and further decreases down to 2699 cm^{-1} when 3 ML of Si are deposited. A further effect, evident by the comparison of the Raman spectra in Fig 8b, is the splitting of the G peak after the silicon deposition. In fact, as summarized in Figure 8e, in the bare epitaxial graphene sample, the Raman shift of the G mode ranges from 1595 cm^{-1} to 1605 cm^{-1}, while after the Si deposition is possible to define G^+ and G^- Raman modes; in case of 1 ML of Si the G^+ and G^- modes range from 1596 cm^{-1} and 1580 cm^{-1} to 1602 cm^{-1} and 1583 cm^{-1}, respectively. When 3 Si MLs are deposited the ranges of the G^+ and G^- modes are slightly modified (G^+ from 1600 cm^{-1} to 1605 cm^{-1} and G^- from 1579 cm^{-1} to 1583 cm^{-1}). The presence of the splitting of the G peak and the 2D downshift are a

clear evidence of a tensile strain affecting the epitaxial graphene layer. [39] In addition, from the analysis of the G^+ and G^- distance, we can infer that the graphene layer is subjected to a tensile strain of about 0.5 % after silicon deposition. This result is consistent with the Raman spectra observed for silicene nanosheets intercalated under the outermost carbon atom layer of a HOPG substrate reported in ref. [20], where a density functional theory calculation demonstrated that a graphene layer on the silicene nanosheet suffers a tensile strain ranging from 0 to 4 % of the graphene lattice parameter.[20] The last effect evolution of the Raman spectra presented in Figure 8b is the increase in intensity of the D peak, related to the intervalley phonon and defect scattering. In fact, in the spectrum of the bare epi-Gr, the D peak is low but detectable, while after the deposition of silicon an evident peak appears. Considering the splitting of the G peak after Si deposition it is difficult to assess from the D/G intensity ratio, that is reported in Figure SM6, a detailed evaluation of the defect concentration. Nonetheless, this is not the case for the pristine epi-Gr substrate, for which the D/G intensity ratio reaches values up to 0.25, corresponding to a defect concentration of 5.6×10^{10} cm^{-2} or equivalently to an average distance, L_D, between defects of about 24 nm. [40] All the graphene Raman maps are reported in Figure SM7.

Discussion

In the present work, both the XPS and STM measurements indicate room temperature Si intercalation under the epi-Gr layer. Although graphene is known to be one of the least permeable materials because of its very small first neighbor distance in the atomic network, intercalation of Si atoms deposited on its surface at room temperature has previously been observed and suggested to be driven by a diffusion mechanism through the graphene defects. [25, 28] First principle calculations show that a Si atom needs at least 3 eV to penetrate the ideal graphene network. [41] Si atoms are deposited by thermal evaporation, reaching the graphene surface at temperatures very close to RT, i.e. with energies of the order of 0.025eV. These experimental conditions hamper any Si atom intercalation at RT. In ref. 25, ab-initio calculations showed that in presence of carbon atom vacancies in the free-standing graphene network, the intercalation process occurs in two steps. First the Si atom tends to repair the vacancy, by substituting to the missing atom or covalently binding above the defect, then only if the Si atom has an energy of about 0.5 eV, it can penetrate the graphene sheet. A similar energy value has been obtained by Li et al. [42] , who also reported the substrate role in lowering to 0.33 eV the Si atom energy required for its intercalation under the epi-Gr on the Ru(0001) surface. On the other hand, it is well known that there is an energetic gain upon atom adsorption on a surface. This energy is initially absorbed as vibrational energy of the system adatom/substrate, then it is released in a few ps through several channels, e.g. phonon dissipation, adatom diffusion on the surface, interaction by reacting with the surface atoms forming an alloy or intercalation. [43] This surplus energy has been calculated, in the case of a Si atom on free standing graphene, to be between 0.1 and 0.8 eV depending on the Si adsorption site and between 0.5 and 2.3 eV in the presence of epi-Gr on a Ni(111) substrate. [25] This means that in the

presence of a graphene vacancy, Si atoms have enough energy to intercalate under the epi-Gr network even at RT. The presence of defects on the pristine epi-Gr is imaged in Figure SM3 and confirmed over a more extended area by Raman analysis (see Figure SM6) proving that the D/G intensity ratio for the pristine epi-Gr reaches values up to 0.25, corresponding to an underestimated average distance of about 24 nm between epi-Gr point defects. Such a defect amount, though low, could be sufficient to induce Si atom intercalation mechanism. In addition, it has been reported that the presence of Si adsorbates on epi-Gr hugely reduces the energy required for graphene defect formation. [42] This can allow an increase of epi-Gr defects upon Si adsorption and can further increase the epi-Gr sites available for Si atom intercalation, thus explaining the enhancement of the D/G intensity ratio for 1 ML and 3 ML Si deposition (see Figure SM6) as well as the average distance between Si nanostructures (see e.g. the STM image in Figure 3a) well lower than the L_D value of 24 nm estimated from the D/G intensity ratio. Very recently, silicene formation only on top of the epi-Gr surface has been demonstrated to occur for a pristine almost ideal epi-Gr. [30] Indeed, in that case, the very low D/G intensity ratio value of 0.09 has been attributed to a D peak intensity mostly due to the intervalley phonon scattering induced by the observed overall presence of epi-Gr/BL armchair step edges, [30, 34] thus reducing much the defect amount concentration on the epi-Gr so preventing from Si atom intercalation. For 1 ML of Si deposition, the STM images show the formation under the graphene network of Si nanostructures with lateral extension up to 10 nm, while no evidence of Si crystalline or amorphous three-dimensional clusters on the epi-Gr surface is detected. From STM analyses no straightforward indication on the structural order of these Si intercalated nanostructures can be obtained. Nonetheless, STS measurements indicate a full decoupling between the epi-Gr and the intercalated Si atoms underneath (see the resemblance between the red and black curves in Figure 6), therefore suggesting the absence of chemical bonds between the Si and C atoms of the epi-Gr. In the 3 ML case, the sample surface is covered by three-dimensional islands of various sizes, with a semiconducting nature as displayed by STS measurements. The Raman spectra of the 1ML and 3ML cases, present peaks at 538 cm^{-1} and 532 cm^{-1}, respectively. These Raman modes are very close to the one located around 542 cm^{-1}, reported for Si deposited on HOPG substrate and attributed to silicene nanosheets with 0.05 nm buckling and 0.228 nm average bond length. [19] The theoretical Raman mode has been calculated to be around 577 cm^{-1} for free-standing flat silicene and to shift toward lower wavenumber with silicene buckling increasing. [44] Elongation of Si atom bond lengths (with constant buckling) has also been reported to lead to an even more pronounced silicene Raman mode redshift. [19] On the other hand, it has been theoretically predicted that the finite size of silicene sheets on a HOPG surface gives rise to an extension of the Si-Si bond length due to the removal of periodic constraints with respect to the interfaces, leading to a redshift to about 542-550 cm^{-1}. [19] In this framework, the shift of the present Raman modes could be due to a further small lengthening of the Si atom bond length and/or to the charge transfer between the BL and the silicene nanosheets as discussed in the Results section. [45] The histogram of the 2D silicon Raman intensity (Figure 7b) shows a single peak distribution for 1 ML case and a three peaks distribution for the 3 ML. This

can be interpreted as a silicene bilayer formation or/and as the presence of regions where the density of surface occupied by the silicene is higher. Considering the STM observation, this is consistent with the formation of silicene nanosheets with lateral dimensions up to 10 nm (instead of a continuous intercalated 2D layer) with several of them integrated on the Raman maps (since each pixel of the map counts signals from a 500 nm x 500 nm area). So, increasing the number of silicene nanosheets in the pixel area, increases the Raman peak intensity. Raman maps highlight silicene area random distribution for 1 ML case, whereas they give a hint for higher silicene Raman mode intensities along certain directions, which are likely to correspond to the step-edges of the SiC substrates. This is a further indication of the role played by the defects (namely, atomic vacancies, dislocations, graphene sheet borders, step edges, …) in the Si intercalation under the epi-Gr layer, as already reported in the case of Si deposition at RT on epi-Gr/Ni(111) system. [25] Differently from this last system and from the Si deposition at RT on HOPG substrate, for the 1 ML case, the absence of Raman modes located at 520 cm^{-1} and around 470 cm^{-1} attested the absence of formation of 3D crystalline and of amorphous Si structures. This result could be tentatively attributed to the higher amount of defects present in our epi-Gr with respect to the one on the epi-Gr grown on a Ni(111) substrate or on the bare HOPG surface, [19, 20] thus making Si intercalation energetically more favorable than Si diffusion and aggregation on the epi-Gr surface at low Si coverages. When the Si deposited reaches 3ML, both adsorption energy releasing mechanisms are active, giving rise to intercalation of Si atoms under the epi-Gr layer and diffusion on the surface with formation of 3D semiconducting (see the STS differential conductance reported in Figure 6, blue curve) and amorphous nanostructures, as illustrated by the absence of sharp LEED pattern detection and Raman spectra. Eventually, for both Si coverages, Raman analyses in the graphene mode region show evidence for the splitting of the G mode into two bands G^+ and G^- and a redshift of the 2D mode. This effect has been reported to be due to tensile strain experienced by the graphene layer. [39] From the analysis of the distance between G^+ and G^- peak positions, we can infer that the graphene layer suffered an average tensile strain of about 0.5 % after silicon deposition. This result is consistent with the Raman spectra observed for silicene nanosheets intercalated under the outermost carbon atom layer of a HOPG substrate reported in ref. [20] where a density functional theory calculation demonstrated that a graphene layer on the silicene nanosheet suffers a tensile strain ranging from 0 to 4 % of the graphene lattice parameter, with the highest amount of strain (1-4%) located only close to the edge of the silicene nanosheet and at the most external border of the resulting graphene bump and strain values between 0 and 1% elsewhere. [20]

Conclusions

In the present work, for 1 ML Si coverage, XPS and STM measurements indicate Si intercalation under the epi-Gr layer, forming nanometric-sized structures. All observed nanosheets exhibit a surface lattice network and STS differential conductance similar to that of non-intercalated epi-Gr nearby. The occurrence of the intercalation process is corroborated also by Raman measurements assessing: i) the splitting of the G band

and the 2D downshift, both indicating the presence of a tensile strain on the epi-Gr layer and ii) the 2D broadening as well as the D feature intensity increase, pointing out the increase of sp^3 hybridization in the epi-Gr layer. At the same time, Raman spectra show the occurrence of well-defined features at 538 cm^{-1} and 532 cm^{-1} for the 1 ML and 3 ML cases, respectively, very close to the ones already ascribed to low-buckled silicene nanosheets. All these results constitute a body of evidence to conclude that silicene nanosheets form at RT under the epi-Gr layer and are all consistent with the presence of defects (e.g. atomic vacancies, dislocations, step and graphene sheet edges, …) on the pristine epi-Gr network as measured by Raman spectroscopy revealing, a D/G band intensity ratio reaching values up to 0.25. In addition, these outcomes open an avenue to control the RT synthesis of more extended intercalated silicene layers on SiC(0001) substrate through pristine epi-Gr defect concentration managing and silicene/graphene vertical junction application in nanotechnology.

Acknowledgements

P.C., M. D.C., M.S and M.S. would like to acknowledge the European Community for the HORIZON2020 MSC-RISE Project DiSeTCom (GA 823728). HV would like to acknowledge the HPC centers of IDRIS (Grant A0080900642) and CERMM for computational resources.

References

1. Aeschlimann, S.; Rossi, A.; Chavez-Cervantes, M.; Krause, R.; Arnoldi, B.; Stadtmuller, B.; Aeschlimann, M.; Forti, S.; Fabbri, F.; Coletti, C.; Gierz, I., Direct evidence for efficient ultrafast charge separation in epitaxial WS2/graphene heterostructures. *Sci Adv* **2020,** *6* (20), aay0761.
2. Fabbri, F.; Dinelli, F.; Forti, S.; Sementa, L.; Pace, S.; Piccinini, G.; Fortunelli, A.; Coletti, C.; Pingue, P., Edge Defects Promoted Oxidation of Monolayer WS2 Synthesized on Epitaxial Graphene. *J Phys Chem C* **2020,** *124* (16), 9035-9044.
3. Liu, X. L.; Balla, I.; Bergeron, H.; Campbell, G. P.; Bedzyk, M. J.; Hersam, M. C., Rotationally Commensurate Growth of MoS2 on Epitaxial Graphene. *Acs Nano* **2016,** *10* (1), 1067-1075.
4. Al Balushi, Z. Y.; Wang, K.; Ghosh, R. K.; Vila, R. A.; Eichfeld, S. M.; Caldwell, J. D.; Qin, X. Y.; Lin, Y. C.; DeSario, P. A.; Stone, G.; Subramanian, S.; Paul, D. F.; Wallace, R. M.; Datta, S.; Redwing, J. M.; Robinson, J. A., Two-dimensional gallium nitride realized via graphene encapsulation. *Nat Mater* **2016,** *15* (11), 1166-1171.
5. Pecz, B.; Nicotra, G.; Giannazzo, F.; Yakimova, R.; Koos, A.; Kakanakova-Georgieva, A., Indium Nitride at the 2D Limit. *Adv Mater* **2021,** *33* (1).
6. Forti, S.; Stohr, A.; Zakharov, A. A.; Coletti, C.; Emtsev, K. V.; Starke, U., Mini-Dirac cones in the band structure of a copper intercalated epitaxial graphene superlattice. *2d Mater* **2016,** *3* (3), 035003.
7. Forti, S.; Link, S.; Stohr, A.; Niu, Y. R.; Zakharov, A. A.; Coletti, C.; Starke, U., Semiconductor to metal transition in two-dimensional gold and its van der Waals heterostack with graphene. *Nat Commun* **2020,** *11* (1), 2236.
8. *Silicene. Structure, Properties and Applications* Springer, Cham: 2016; p XVI, 276.

9. Cahangirov, S.; Topsakal, M.; Akturk, E.; Sahin, H.; Ciraci, S., Two- and One-Dimensional Honeycomb Structures of Silicon and Germanium. *Phys Rev Lett* **2009,** *102* (23), 236804.
10. Le Lay, G., 2D MATERIALS Silicene transistors. *Nat Nanotechnol* **2015,** *10* (3), 202-203.
11. Wang, Y. Y.; Ni, Z. Y.; Liu, Q. H.; Quhe, R. G.; Zheng, J. X.; Ye, M.; Yu, D. P.; Shi, J. J.; Yang, J. B.; Li, J.; Lu, J., All-Metallic Vertical Transistors Based on Stacked Dirac Materials. *Adv Funct Mater* **2015,** *25* (1), 68-77.
12. Vogt, P.; De Padova, P.; Quaresima, C.; Avila, J.; Frantzeskakis, E.; Asensio, M. C.; Resta, A.; Ealet, B.; Le Lay, G., Silicene: Compelling Experimental Evidence for Graphenelike Two-Dimensional Silicon. *Phys Rev Lett* **2012,** *108* (15), 155501.
13. Tao, L.; Cinquanta, E.; Chiappe, D.; Grazianetti, C.; Fanciulli, M.; Dubey, M.; Molle, A.; Akinwande, D., Silicene field-effect transistors operating at room temperature. *Nat Nanotechnol* **2015,** *10* (3), 227-231.
14. Meng, L.; Wang, Y. L.; Zhang, L. Z.; Du, S. X.; Wu, R. T.; Li, L. F.; Zhang, Y.; Li, G.; Zhou, H. T.; Hofer, W. A.; Gao, H. J., Buckled Silicene Formation on Ir(111). *Nano Lett* **2013,** *13* (2), 685-690.
15. Huang, L.; Zhang, Y. F.; Zhang, Y. Y.; Xu, W. Y.; Que, Y. D.; Li, E.; Pan, J. B.; Wang, Y. L.; Liu, Y. Q.; Du, S. X.; Pantelides, S. T.; Gao, H. J., Sequence of Silicon Monolayer Structures Grown on a Ru Surface: from a Herringbone Structure to Silicene. *Nano Lett* **2017,** *17* (2), 1161-1166.
16. Chiappe, D.; Scalise, E.; Cinquanta, E.; Grazianetti, C.; van den Broek, B.; Fanciulli, M.; Houssa, M.; Molle, A., Two-Dimensional Si Nanosheets with Local Hexagonal Structure on a MoS2 Surface. *Adv Mater* **2014,** *26* (13), 2096-2101.
17. van Bremen, R.; Yao, Q. R.; Banerjee, S.; Cakir, D.; Oncel, N.; Zandvliet, H. J. W., Intercalation of Si between MoS2 layers. *Beilstein J Nanotech* **2017,** *8*, 1952-1960.
18. De Crescenzi, M.; Berbezier, I.; Scarselli, M.; Castrucci, P.; Abbarchi, M.; Ronda, A.; Jardali, F.; Park, J.; Vach, H., Formation of Silicene Nanosheets on Graphite. *Acs Nano* **2016,** *10* (12), 11163-11171.
19. Castrucci, P.; Fabbri, F.; Delise, T.; Scarselli, M.; Salvato, M.; Pascale, S.; Francini, R.; Berbezier, I.; Lechner, C.; Jardali, F.; Vach, H.; De Crescenzi, M., Raman investigation of air-stable silicene nanosheets on an inert graphite surface. *Nano Res* **2018,** *11* (11), 5879-5889.
20. Kupchak, I.; Fabbri, F.; De Crescenzi, M.; Scarselli, M.; Salvato, M.; Delise, T.; Berbezier, I.; Pulci, O.; Castrucci, P., Scanning tunneling microscopy and Raman evidence of silicene nanosheets intercalated into graphite surfaces at room temperature. *Nanoscale* **2019,** *11* (13), 6145-6152.
21. Sone, J.; Yamagami, T.; Nakatsuji, K.; Hirayama, H., Si growth at graphene surfaces on 6H-SiC(0001) substrates. *Jpn J Appl Phys* **2016,** *55* (3), 035502.
22. Mao, J. H.; Huang, L.; Pan, Y.; Gao, M.; He, J. F.; Zhou, H. T.; Guo, H. M.; Tian, Y.; Zou, Q.; Zhang, L. Z.; Zhang, H. G.; Wang, Y. L.; Du, S. X.; Zhou, X. J.; Castro Neto, A. H.; Gao, H. J., Silicon layer intercalation of centimeter-scale, epitaxially grown monolayer graphene on Ru(0001). *Appl Phys Lett* **2012,** *100* (9), 093101.
23. Jardali, F.; Lechner, C.; De Crescenzi, M.; Scarselli, M.; Berbezier, I.; Castrucci, P.; Vach, H., The potentially crucial role of quasi-particle interferences for the growth of silicene on graphite. *Nano Res* **2020,** *13* (9), 2378-2383.
24. Cai, Y.; Chuu, C. P.; Wei, C. M.; Chou, M. Y., Stability and electronic properties of two-dimensional silicene and germanene on graphene. *Phys Rev B* **2013,** *88* (24), 245408.
25. Ronci, F.; Colonna, S.; Flammini, R.; De Crescenzi, M.; Scarselli, M.; Salvato, M.; Berbezier, I.; Jardali, F.; Lechner, C.; Pochet, P.; Vach, H.; Castrucci, P., High graphene permeability for room temperature silicon deposition: The role of defects. *Carbon* **2020,** *158*, 631-641.
26. Satta, M.; Colonna, S.; Flammini, R.; Cricenti, A.; Ronci, F., Silicon Reactivity at the Ag(111) Surface. *Phys Rev Lett* **2015,** *115* (2), 026102.
27. Xia, C.; Watcharinyanon, S.; Zakharov, A. A.; Yakimova, R.; Hultman, L.; Johansson, L. I.; Virojanadara, C., Si intercalation/deintercalation of graphene on 6H-SiC(0001). *Phys Rev B* **2012,** *85* (4), 045418.
28. Visikovskiy, A.; Kimoto, S.; Kajiwara, T.; Yoshimura, M.; Iimori, T.; Komori, F.; Tanaka, S., Graphene/SiC(0001) interface structures induced by Si intercalation and their influence on electronic properties of graphene. *Phys Rev B* **2016,** *94* (24), 245421.
29. Matusalem, F.; Koda, D. S.; Bechstedt, F.; Marques, M.; Teles, L. K., Deposition of topological silicene, germanene and stanene on graphene-covered SiC substrates. *Sci Rep-Uk* **2017,** *7*, 15700.

30. Ben Jabra, Z.; Abel, M.; Fabbri, F.; Aqua, J.-N.; Koudia, M.; Michon, A.; Castrucci, P.; Ronda, A.; Vach, H.; De Crescenzi, M.; Berbezier, I., Van der Waals heteroepitaxy of air-stable quasi-free-standing silicene layers on CVD epitaxial graphene/6H-SiC. *Acs Nano* **2022**.
31. Mammadov, S.; Ristein, J.; Koch, R. J.; Ostler, M.; Raidel, C.; Wanke, M.; Vasiliauskas, R.; Yakimova, R.; Seyller, T., Polarization doping of graphene on silicon carbide. *2d Mater* **2014,** *1* (3), 035003.
32. Giambra, M. A.; Miseikus, V.; Pezzini, S.; Marconi, S.; Montanaro, A.; Fabbri, F.; Sorianello, V.; Ferrari, A. C.; Coletti, C.; Romagnoli, M., Wafer-Scale Integration of Graphene-Based Photonic Devices. *Acs Nano* **2021,** *15* (2), 3171-3187.
33. Riedl, C.; Coletti, C.; Starke, U., Structural and electronic properties of epitaxial graphene on SiC(0 0 0 1): a review of growth, characterization, transfer doping and hydrogen intercalation. *J Phys D Appl Phys* **2010,** *43* (37), 374009.
34. Ben Jabra, Z.; Berbezier, I.; Michon, A.; Koudia, M.; Assaf, E.; Ronda, A.; Castrucci, P.; De Crescenzi, M.; Vach, H.; Abel, M., Hydrogen-Mediated CVD Epitaxy of Graphene on SiC: Implications for Microelectronic Applications. *Acs Appl Nano Mater* **2021,** *4* (5), 4462-4473.
35. Goler, S.; Coletti, C.; Piazza, V.; Pingue, P.; Colangelo, F.; Pellegrini, V.; Emtsev, K. V.; Forti, S.; Starke, U.; Beltram, F.; Heun, S., Revealing the atomic structure of the buffer layer between SiC(0001) and epitaxial graphene. *Carbon* **2013,** *51*, 249-254.
36. Riedl, C.; Starke, U.; Bernhardt, J.; Franke, M.; Heinz, K., Structural properties of the graphene-SiC(0001) interface as a key for the preparation of homogeneous large-terrace graphene surfaces. *Phys Rev B* **2007,** *76* (24), 245406.
37. Yan, J. A.; Stein, R.; Schaefer, D. M.; Wang, X. Q.; Chou, M. Y., Electron-phonon coupling in two-dimensional silicene and germanene. *Phys Rev B* **2013,** *88* (12), 121403(R).
38. Ferrari, A. C.; Meyer, J. C.; Scardaci, V.; Casiraghi, C.; Lazzeri, M.; Mauri, F.; Piscanec, S.; Jiang, D.; Novoselov, K. S.; Roth, S.; Geim, A. K., Raman spectrum of graphene and graphene layers. *Phys Rev Lett* **2006,** *97* (18), 187401
39. Mohiuddin, T. M. G.; Lombardo, A.; Nair, R. R.; Bonetti, A.; Savini, G.; Jalil, R.; Bonini, N.; Basko, D. M.; Galiotis, C.; Marzari, N.; Novoselov, K. S.; Geim, A. K.; Ferrari, A. C., Uniaxial strain in graphene by Raman spectroscopy: G peak splitting, Gruneisen parameters, and sample orientation. *Phys Rev B* **2009,** *79* (20), 205433.
40. Cancado, L. G.; Jorio, A.; Ferreira, E. H. M.; Stavale, F.; Achete, C. A.; Capaz, R. B.; Moutinho, M. V. O.; Lombardo, A.; Kulmala, T. S.; Ferrari, A. C., Quantifying Defects in Graphene via Raman Spectroscopy at Different Excitation Energies. *Nano Lett* **2011,** *11* (8), 3190-3196.
41. Cui, Y.; Gao, J. F.; Jin, L.; Zhao, J. J.; Tan, D. L.; Fu, Q.; Bao, X. H., An Exchange Intercalation Mechanism for the Formation of a Two-Dimensional Si Structure Underneath Graphene. *Nano Res* **2012,** *5* (5), 352-360.
42. Li, G.; Zhou, H. T.; Pan, L. D.; Zhang, Y.; Huang, L.; Xu, W. Y.; Du, S. X.; Ouyang, M.; Ferrari, A. C.; Gao, H. J., Role of Cooperative Interactions in the Intercalation of Heteroatoms between Graphene and a Metal Substrate. *J Am Chem Soc* **2015,** *137* (22), 7099-7103.
43. Meyer, J.; Reuter, K., Modeling Heat Dissipation at the Nanoscale: An Embedding Approach for Chemical Reaction Dynamics on Metal Surfaces. *Angew Chem Int Edit* **2014,** *53* (18), 4721-4724.
44. Scalise, E.; Cinquanta, E.; Houssa, M.; van den Broek, B.; Chiappe, D.; Grazianetti, C.; Pourtois, G.; Ealet, B.; Molle, A.; Fanciulli, M.; Afanas'ev, V. V.; Stesmans, A., Vibrational properties of epitaxial silicene layers on (111) Ag. *Appl Surf Sci* **2014,** *291*, 113-117.
45. Riedl, C.; Coletti, C.; Iwasaki, T.; Zakharov, A. A.; Starke, U., Quasi-Free-Standing Epitaxial Graphene on SiC Obtained by Hydrogen Intercalation. *Phys Rev Lett* **2009,** *103* (24), 246804.